Purdue University
Purdue e-Pubs

International Compressor Engineering Conference   School of Mechanical Engineering

2014

Wave Propagation in a Radial Duct with Mean Swirling Flow

Yujun Leng
Purdue University, West Lafayette, United States of America, leng@purdue.edu

Sanford Fleeter
Purdue University, West Lafayette, United States of America, fleeter@purdue.edu

Follow this and additional works at: https://docs.lib.purdue.edu/icec

Analytical Modeling of the Unsteady Wave Propagation in the Vaneless Space of a Low Speed Centrifugal Compressor

Yujun LENG[1]*, Sanford FLEETER[2]

[1]Purdue University, School of Mechanical Engineering,
West Lafayette, Indiana, USA
leng@purdue.edu

[2]Purdue University, School of Mechanical Engineering,
West Lafayette, Indiana, USA
fleeter@purdue.edu

* Corresponding Author

ABSTRACT

An analytical model is developed to predict the propagation of unsteady pressure and vorticity waves in the vaneless space of a low speed centrifugal compressor. The flow is assumed to be an inviscid isentropic two-dimensional flow in the radial and circumferential directions at low Mach number. Results analyze the effects of the mean flow field and circumferential wavenumber on the propagating behavior of the unsteady pressure and vorticity waves. These unsteady waves are the links in the analysis of unsteady impeller diffuser vane interaction. The analytical solution provides a quick and physically insightful means of understanding unsteady impeller diffuser vane interactions.

1. INTRODUCTION

Traditionally, centrifugal compressors have relatively fewer aeromechanic issues as compared to axial compressors. However, in recent years, effort is being directed at developing the next generation high power density centrifugal compressors. In these advanced designs, a vaned diffuser is frequently used to increase the compressor efficiency. The vaneless space between the impeller exit and vaned diffuser is small so as to increase the diffuser's performance. However, the impeller wakes hitting the diffuser vanes generate a series of strong pressure waves which propagate upstream and affect the impeller trailing edge. Both experimental (König *et al.,* 2009) and computational simulations (Ramakrishnan *et al.*, 2011) have shown that under certain operating conditions, these pressure waves generated from the impeller-diffuser vane interaction are large enough to cause impeller failure. Bryan (1991) investigated unsteady impeller-diffuser interactions in the Purdue Low-Speed Centrifugal Research Compressor. Gottfried and Fleeter (2002) developed a small perturbation model to predict the unsteady aerodynamic response of impeller blades to the diffuser vane potential field. However, there is no analytical model developed to predict the impeller excitation by the pressure wave resulting from the impeller wake -diffuser vane interactions.

To analyze this aeromechanic risk, three major physical processes have to be understood, Figure 1: (1) the impeller wake travels downstream; (2) the wake interacts with the diffuser vane and generates the pressure waves; (3) the pressure wave travels upstream and excites the impeller. This paper focuses on modeling process 1 and 3, i.e. developing an analytical model and solution for the wake and pressure wave propagation in the vaneless space with a mean swirling flow. These wave propagation properties are also fundamental to the linearized modeling of the unsteady aerodynamics in radial cascades, process 2.
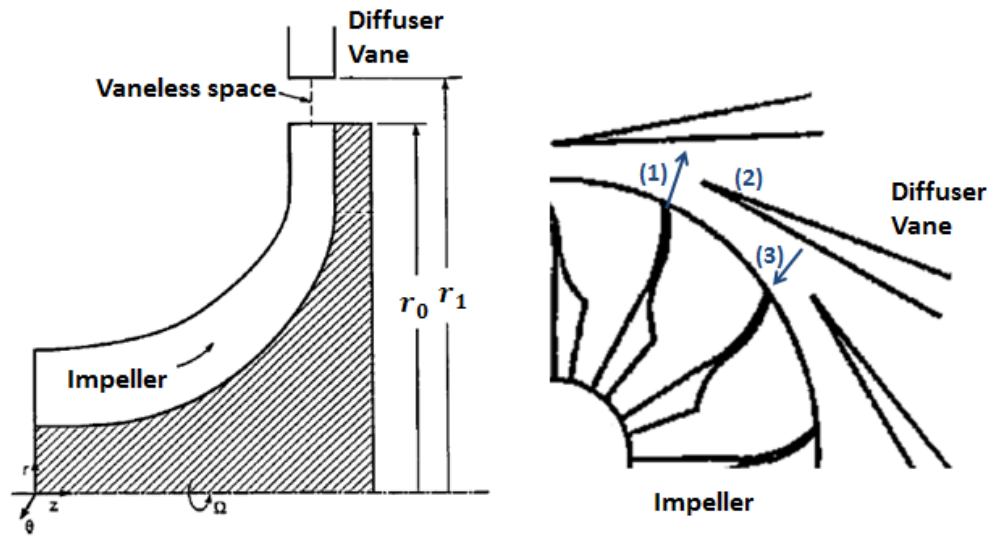
Figure 1: Schematic of a centrifugal compressor (Gottfried and Fleeter (2002))

2. ANALYTICAL MODEL

In subsonic centrifugal compressors, the vaneless space between the impeller and the vaned diffuser is usually in the shape of a thin annulus. The flow field can be modeled as a non-uniform steady mean flow with unsteady pressure and vorticity waves. This study is directed at the analytical modeling to quantify the propagating behavior of these unsteady waves. To reduce the complexity of the problem, the flow is assumed to be an inviscid isentropic two-dimensional flow in the radial and circumferential directions.

2.1 Governing Equations
The flow field is described by the Euler equations:

$$\frac{\partial \rho}{\partial t} + (\vec{U} \cdot \nabla)\rho + \rho \nabla \cdot \vec{U} = 0 \tag{1}$$

$$\frac{\partial \vec{U}}{\partial t} + \vec{U} \cdot \nabla \vec{U} = -\frac{\nabla p}{\rho} \tag{2}$$

The unsteady flow is considered to be a small perturbation to the mean flow.

$$\vec{U} = \vec{U}_0 + \vec{u}$$
$$p = p_0 + p'$$
$$\rho = \rho_0 + \rho' \tag{3}$$

where $\vec{U}_0$, p_0 and ρ_0 are the steady mean velocity, pressure and density. $\vec{u}$, p' and ρ' are the corresponding unsteady perturbation quantities.

The linearized Euler equations are obtained by substituting Equation (3) into Equations (1) and (2). The steady flow is described by Equations (4) and (5), with the small perturbation unsteady flow by Equations (6) and (7)

$$(\vec{U}_0 \cdot \nabla)\rho_0 + \rho_0 \nabla \cdot \vec{U}_0 = 0 \tag{4}$$

$$\vec{U}_0 \cdot \nabla \vec{U}_0 = -\frac{\nabla p_0}{\rho_0} \tag{5}$$

$$\frac{D_0}{Dt}\left(\frac{p'}{\rho_0 a_0^2}\right) + \frac{1}{\rho_0} \nabla \cdot (\rho_0 \vec{u}) = 0 \tag{6}$$

$$\frac{D_0 \vec{u}}{Dt} + \vec{u} \cdot \nabla \vec{U}_0 = -\nabla(\frac{p'}{\rho_0}) \tag{7}$$

where a_0 is the sound speed and $\frac{D_0}{Dt} \equiv \frac{\partial}{\partial t} + \vec{U}_0 \cdot \nabla$ is the convective material derivative.
In addition, for an isentropic process

$$a_0^2 = \frac{\partial p}{\partial \rho} \tag{8}$$

After linearization,

$$\frac{\partial p_0}{\partial r} = a_0^2 \frac{\partial \rho_0}{\partial r} \tag{9}$$

$$\frac{\partial p'}{\partial r} = a_0^2 \frac{\partial \rho'}{\partial r} \tag{10}$$

2.2 Mean Flow field

In 2-D cylindrical coordinates and assuming the mean flow is axisymmetric, i.e. $\frac{\partial}{\partial \theta} = 0$, the continuity and momentum equations, Equations (4) and (5), are

$$\frac{\rho_0}{r} U_{r0} + U_{r0} \frac{\partial \rho_0}{\partial r} + \rho_0 \frac{\partial U_{r0}}{\partial r} = 0 \tag{11}$$

$$U_{r0} \frac{\partial U_{r0}}{\partial r} - \frac{U_{\theta 0}^2}{r} = -\frac{1}{\rho_0} \frac{\partial p_0}{\partial r} \tag{12}$$

$$\frac{\partial U_{\theta 0}}{\partial r} = -\frac{U_{\theta 0}}{r} \tag{13}$$

Integrating Equation (13) yields the mean flow circumferential velocity.

$$U_{\theta 0} = \frac{c_2}{r} \tag{14}$$

where c_2 is a constant.

Equation 13 is valid for a compressible flow and implies that the mean flow is irrotational since

$$\nabla \times \vec{U}_0 = \frac{1}{r}\left(\frac{\partial(r U_{\theta 0})}{\partial r} - \frac{\partial U_{r0}}{\partial \theta}\right)\hat{e}_z = \left(\frac{U_{\theta 0}}{r} + \frac{\partial U_{\theta 0}}{\partial r}\right)\hat{e}_z = 0 \tag{15}$$

Since this analysis is intended for low speed centrifugal compressors, two additional assumptions can be made. First, the mean flow density is assumed to be nearly constant in the vaneless space, i.e. $\frac{\partial \rho_0}{\partial r} = 0$. Second, the square of the mean flow Mach number is neglected. These two assumptions are valid for centrifugal compressors with low impeller exit Mach numbers.

With these assumptions, Equation (11) becomes,

$$\frac{U_{r0}}{r} + \frac{\partial U_{r0}}{\partial r} = 0 \tag{16}$$

Integrating Equation (16) yields the mean flow radial velocity

$$U_{r0} = \frac{c_1}{r} \tag{17}$$

where c_1 is a constant.

Substituting Equations (14) and (17) into Equation (12) gives

$$\frac{\partial p_0}{\partial r} = \rho_0(\frac{c_1^2}{r^3} + \frac{c_2^2}{r^3}) \tag{18}$$

Integrating Equation (18) yields the mean flow pressure.

$$p_0 = -\frac{\rho_0}{2r^2}(c_1{}^2 + c_2{}^2) + c_3 \tag{19}$$

where c_3 is a constant.

2.3 Unsteady Flow Field

The linearized 2D Euler equations, Equations (6) and (7), are the governing equations for the unsteady flow field. As shown by Goldstein (1978), when the mean flow is irrotational (Equation (15)), the pressure wave and vorticity waves, i.e. the impeller wake, are uncoupled. Therefore, use Goldstein's splitting method $\vec{u} = \vec{u}_a + \vec{u}_v$, where $\vec{u}_a$ is the potential part related to the pressure wave and $\vec{u}_v$ is the vortical part related to the vorticity wave. Substituting $\vec{u} = \vec{u}_a + \vec{u}_v$ into Equation (6) and (7), uncouples the pressure and vorticity waves.

The pressure wave governing equations are,

$$\frac{D_0}{Dt}\left(\frac{p'}{\rho_0 a_0^2}\right) + \frac{1}{\rho_0}\nabla \cdot (\rho_0\vec{u}_a) = 0 \tag{20}$$

$$\frac{D_0\vec{u}_a}{Dt} + \vec{u}_a \cdot \nabla\vec{U}_0 = -\nabla(\frac{p'}{\rho_0}) \tag{21}$$

The vorticity wave equations are,

$$\frac{D_0}{Dt}\left(\frac{p'}{\rho_0 a_0^2}\right) + \frac{1}{\rho_0}\nabla \cdot (\rho_0\vec{u}_a) = -\frac{1}{\rho_0}\nabla \cdot (\rho_0\vec{u}_v) \tag{22}$$

$$\frac{D_0\vec{u}_v}{Dt} + \vec{u}_v \cdot \nabla\vec{U}_0 = 0 \tag{23}$$

These equations are written in terms of the perturbation potential φ, $\vec{u}_a = \nabla\varphi$

The pressure wave equations become,

$$\frac{D_0}{Dt}\left(\frac{1}{a_0^2}\frac{D_0\varphi}{Dt}\right) - \frac{1}{\rho_0}\nabla \cdot (\rho_0\nabla\varphi) = 0 \tag{24}$$

$$p' = -\rho_0\frac{D_0\varphi}{Dt} \tag{25}$$

The vorticity wave equations become,

$$\frac{D_0}{Dt}\left(\frac{1}{a_0^2}\frac{D_0\varphi}{Dt}\right) - \frac{1}{\rho_0}\nabla \cdot (\rho_0\nabla\varphi) = \frac{1}{\rho_0}\nabla \cdot (\rho_0\vec{u}_v) \tag{26}$$

$$\frac{D_0\vec{u}_v}{Dt} + \vec{u}_v \cdot \nabla\vec{U}_0 = 0 \tag{27}$$

To reduce the complexity of the problem and change the PDE to ODE, the unsteady perturbations are assumed to be harmonic in time and in the circumferential direction,

$$q = q(r)\exp(i\omega t + ik_\theta\theta) \tag{28}$$

where q is a perturbation property, i.e. φ, p', u_r or u_θ.

In addition, under the low Mach number assumption made before, the mean flow velocities are $U_{r0} = \frac{c_1}{r}$ and $U_{\theta 0} = \frac{c_2}{r}$ as shown in equation (14) and (17). Thus, the pressure wave equation (24) becomes,

$$\frac{\partial^2\varphi}{\partial r^2} + \left(\frac{1}{r} - \frac{2c_1 i\omega}{ra_0^2}\right)\frac{\partial\varphi}{\partial r} + \left(\frac{\omega^2}{a_0^2} + \frac{2c_2\omega k_\theta}{r^2 a_0^2} - \frac{k_\theta^2}{r^2}\right)\varphi = 0 \tag{29}$$

Equation (29) is second order ODE which can be transferred to a Bessel equation by change of variable. Similar to the derivation by Roger (2004), the solution is a combination of Hankel functions of the first and second kinds.

$$\varphi = Ar^{\frac{c_1\omega i}{a_0^2}}H_v^{(1)}\left(\frac{\omega}{a_0}r\right) + Br^{\frac{c_1\omega i}{a_0^2}}H_v^{(2)}(\frac{\omega}{a_0}r) \tag{30}$$

where A,B are constants and the order $v = \sqrt{k_\theta^2 - \frac{2c_2\omega k_\theta}{a_0^2} - \frac{c_1^2\omega^2}{a_0^4}}$

Since $\vec{u}_a = \nabla\varphi$, the corresponding velocity and pressure perturbations are:

$$u_{ra} = \frac{\partial \varphi}{\partial r} \quad \text{and} \quad u_{\theta a} = \frac{1}{r}\frac{\partial \varphi}{\partial \theta} = \frac{ik_\theta}{r}\varphi \tag{31}$$

$$p' = -\rho_0 \frac{D_0\varphi}{Dt} = -\rho_0(i\omega\varphi + \frac{c_1}{r}\frac{\partial\varphi}{\partial r} + \frac{c_2}{r^2}ik_\theta\varphi) \tag{32}$$

With the same assumptions, the vorticity wave momentum Equation (27) becomes,

$$\frac{\partial u_{\theta v}}{\partial r} + (\frac{i\omega}{c_1}r + \frac{\frac{c_2}{c_1}ik_\theta + 1}{r})u_{\theta v} = 0 \tag{33}$$

$$\frac{\partial u_{rv}}{\partial r} + \left(\frac{i\omega}{c_1}r + \frac{\frac{c_2}{c_1}ik_\theta - 1}{r}\right)u_{rv} = 2\frac{c_2}{c_1}\frac{u_{\theta v}}{r} \tag{34}$$

Equations (33) and (34) are first order ODEs. Their solutions are

$$u_{\theta v} = De^{-\frac{i\omega}{2c_1}r^2 - \frac{c_2 ik_\theta}{c_1}ln(r)}\frac{1}{r} \tag{35}$$

$$u_{rv} = e^{-\frac{i\omega}{2c_1}r^2 - \frac{c_2 ik_\theta}{c_1}ln(r)}(Er - \frac{c_2}{c_1}D\frac{1}{r}) \tag{36}$$

where E, D are constants.

3. CASE STUDIES

The analytical models are used investigate a series of examples based on the geometry and operation parameters of the Purdue Low-Speed Centrifugal Research Compressor (Bryan, 1991). It operates at 1790rpm, the impeller consists of 23 blades, and the impeller exit is at r_0=0.366m. The vaned diffuser has 30 vanes, with the vane leading edge at r_1=0.404m. With a flow coefficient of 0.3, the impeller exit absolute flow angle α is 55.5 degrees, and the relative flow angle β is -62.0 degrees. At the impeller exit, the absolute mean flow radial velocity U_{r0} is 20.6m/s, and the absolute mean flow circumferential velocity $U_{\theta 0}$ is 29.9m/s. This flow condition satisfies the low Mach number assumptions made in this analysis. A schematic of the flow field at impeller exit is shown in Figure 2.
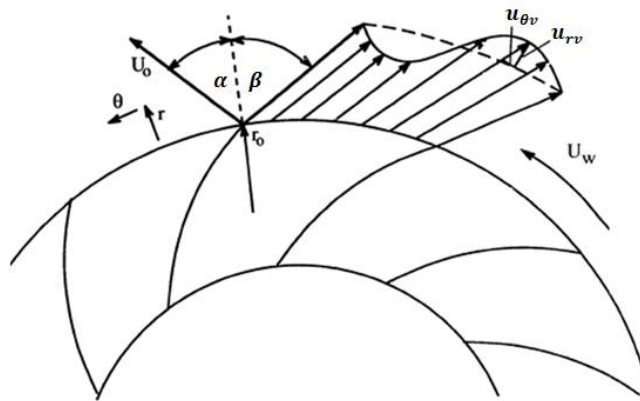

Figure 2: Schematic of the flow field at impeller exit (Bryan (1991))

3.1 Vorticity Wave (Impeller Wake)
Four cases are analyzed to investigate the effect of the number of impeller blades and the relative flow angle on the downstream wake evolution. Case 1 is the base case with 23 blades, α=55.5 degrees and β =-62.0 degrees. In Case 2, the number of blades is reduced to 18, with the flow angles α and β unchanged. In Case 3, the number of blades is increased to 28, with the flow angles α and β unchanged. In Case 4, the relative flow angle is reduced to β =-42.0 degrees, with the absolute flow angle α and the number of blades unchanged. Note that in case 4, due to the reduced back sweep, the mean flow field is changed. At the impeller exit, the absolute mean flow radial velocity U_{r0} is

29.1m/s, and the absolute mean flow circumferential velocity $U_{\theta 0}$ is 42.4m/s. This is approximately 1.4 times the mean flow velocity in the base case.

The unsteady radial or circumferential velocity at impeller exit needs to be specified to calculate the wake propagation downstream. Here it is assumed that the unsteady radial or circumferential velocity are in phase and their amplitude ratio is the same as the mean flow relative radial and circumferential velocity ratio, i.e. $u_{\theta v} = u_{rv} \tan \beta$ at the impeller exit (Figure 2).

The variation of the unsteady circumferential and radial velocities with radius is shown in Figures 3 and 4, with each normalized by their corresponding value at the impeller exit.
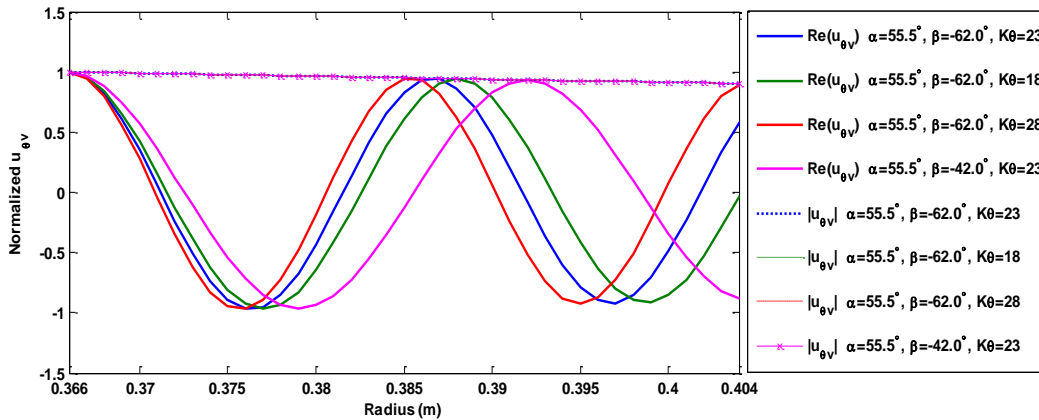

Figure 3: Unsteady circumferential velocity radial profile

As shown in Figure 3, the amplitude of the unsteady circumferential velocity decreases at the same rate for all cases. However, decreasing the number of blades (case 2) and reducing the back sweep angle (case 4) increases the wavelength and decreases the wavenumber in the radial direction. This can also be seen from Equation (35). The amplitude is proportional to 1/r. The equivalent radial wave number can be written as $k_r = -\frac{i\omega}{2c_1}r - \frac{c_2 i k_\theta}{c_1}\frac{\ln(r)}{r}$. Reducing k_θ (case 2) and increasing the mean flow radial velocity constant c_1 (case 4) reduces the wavenumber k_r. Note the equivalent radial wavenumber k_r itself is also a function of radius r.
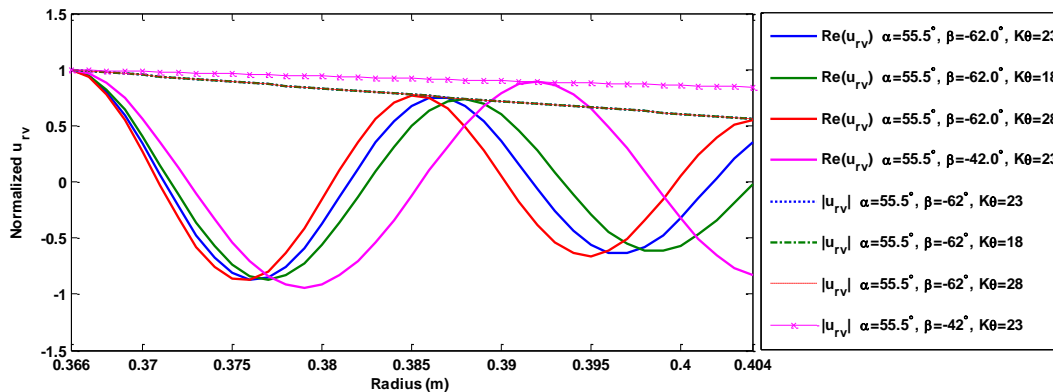

Figure 4: Unsteady radial velocity radial profile

As shown in Figure 4, changing the number of blades does not affect the amplitude of the unsteady radial velocity decay rate. However, reducing the back sweep angle causes the amplitude of the unsteady radial velocity to decay at a slower rate. Regarding the wavelength, the same trends are seen as those observed in the unsteady circumferential velocity: decreasing the number of blades and reducing the back sweep angle increase the wavelength and decrease the wavenumber in the radial direction. From Equation (36), the equivalent radial wavenumber $k_r = -\frac{i\omega}{2c_1}r - \frac{c_2 i k_\theta}{c_1}\frac{\ln(r)}{r}$ stays the same as that for the unsteady circumferential velocity. Physically, both the unsteady radial and

circumferential velocities are from the same vorticity wave, and thus must have the same wave number. The amplitude of the unsteady radial velocity is proportional to $|Er - \frac{c_2}{c_1}D\frac{1}{r}|$. The change in the decay rate in case 4 is due to the assumption that the initial unsteady velocities at the impeller exit are related by the relative flow angle β, $u_{\theta v} = u_{rv}\tan\beta$. Reducing the back sweep angle causes a relatively smaller $u_{\theta v}$ and larger u_{rv}. This causes the change of constants E and D in Equation (36) and thus the change in the amplitude decay rate.

3.2 Pressure Wave

Four case studies are considered to investigate the effect of the circumferential wavenumber k_θ and relative flow angle on the pressure wave propagation upstream from the vaned diffuser due to the impeller wake - diffuser vane interaction. The possible circumferential wavenumber follow the Tyler/Sofrin modes as in axial compressors. (Tyler, 1962)

$$k_\theta = mNB + nNV \tag{37}$$

where NB and NV are the number of blades and vanes number respectively, and m and n are integers.

Three combinations (m,n)=(1,0), (1,-1) and (1,1) are chosen in Cases 1, 2 and 3, respectively. The resulting circumferential wave numbers are $k_\theta = 23$, $k_\theta = -7$ and $k_\theta = 53$ for Cases 1, 2 and 3, with the flow conditions the same as the base case, i.e. α=55.5 degrees and β =-62.0 degrees. In Case 4, $k_\theta = 23$ and α=55.5 degrees stays the same as case 1, but the relative flow angle is reduced to β =-42.0 degrees. As previously discussed, due to the reduced back sweep in Case 4, the mean flow velocity increases to approximately 1.4 times the base case. Figure 5 shows the variation of the pressure wave amplitudes as they propagate from the diffuser vane leading edge to the impeller trailing edge, with the pressure wave amplitudes normalized by their corresponding values at the vaned diffuser leading edge.
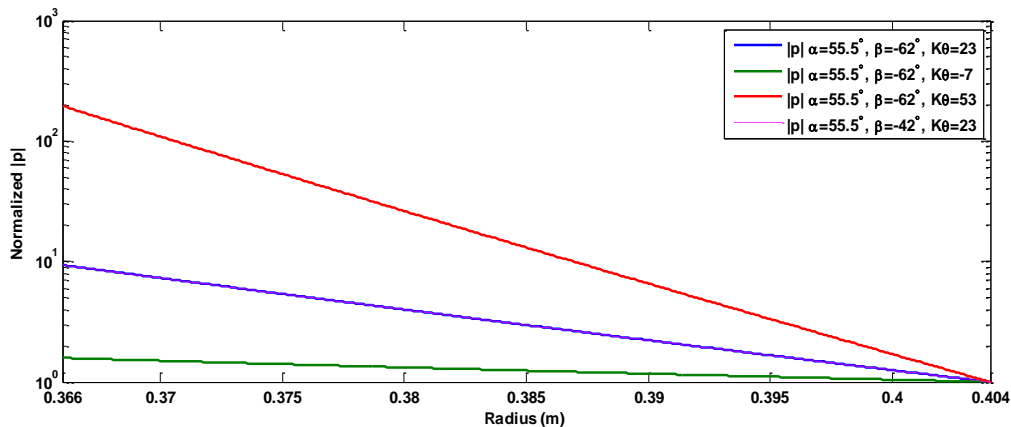

Figure 5: Unsteady pressure wave amplitude profile over radius

Figure 5 shows that as the pressure waves propagate inwardly, their amplitudes all increase due to the space contraction and thus the increase of the acoustic energy density. Larger circumferential wave numbers lead to a higher amplitude growth rate. Comparing Cases 1 and 4, the change in the relative flow angle has a negligible effect on the change of the pressure wave amplitude growth rate.

4. DISCUSSION

4.1 Pressure Wave

As shown in Figure 5, the circumferential wave number change has a large effect on the pressure wave growth rate - the larger the circumferential wave number, the higher the growth rate. This is opposite the trend for axial compressors. Smith (1971) modeled the pressure wave in an axial compressor as the pressure wave travelling in a thin axial annular duct. The results showed that the larger the circumferential wavenumber, the more likely the pressure wave will be cut-off and decay faster in the axial direction. Thus higher order Tyler/Sofrin modes tend to be neglected in acoustics and aeromechanics analyses in axial compressors. This study shows that the higher order

modes may be an important excitation source to the impeller as their amplitude growth is much faster than the lower order modes as it travels inwardly.

4.2 Vorticity Wave (Impeller Wake)
The impeller wake decays in real compressors due to turbulent mixing and viscous effects. With the inviscid flow in this study, the circumferential velocity of the vorticity wave decreases with radius, Equation (35). However, the amplitude of the radial velocity of the vorticity wave is proportional to $|Er - \frac{c_2}{c_1} D \frac{1}{r}|$, Equation (36). As the radius is increased, the amplitude of the unsteady radial velocity increase is proportional to r. In a similar study of vorticity waves in an inviscid axial annular swirling flow, Golubev and Atassi (2000) found a similar algebraic growth of the unsteady axial velocity as it travels downstream. In fact, the divergent behavior of the unsteady wave in swirling flow is well studied in the area of centrifugal instability (Drazin, 2004). In a two dimensional inviscid flow with only a circumferential mean velocity $U_{\theta 0}$, an axisymmetric disturbance, i.e. $k_\theta = 0$, will become unstable when $\frac{\partial(r U_{\theta 0})}{\partial r} < 0$, which is known as Rayleigh's criterion. In this study, $\frac{\partial(r U_{\theta 0})}{\partial r} = 0$ is on the edge of Rayleigh's criterion. However, with a radial mean flow and non-axisymmetric disturbance, the flow field in this study is more complicated. There is no existing stability criterion for the flow field. Note that the model in this research is a linearized model based on small perturbation theory in inviscid flow. In actual compressors, either viscous dissipation or nonlinear effects will mitigate the growth the vorticity amplitude in the radial direction.

For voticity waves, to satisfy the continuity equation (26), there is a hydrodynamic pressure wave induced by the vorticity wave as discussed by Golubev and Atassi (2000). However, Golubev and Atassi (2000) show that the hydrodynamic pressure wave is much weaker than the potential pressure wave governed by Equations (24) and (25). Thus, the hydrodynamic pressure wave is not discussed in this study.

5. CONCLUSIONS

Analytical wave solutions were derived to qualify the inward/outward propagating pressure wave and outward propagating vorticity wave in a radial duct with mean swirling flow. Several case studies were performed to investigate the effects of relative flow angle and circumferential wave number on the propagating behavior of the pressure and vorticity waves. The results of these studies demonstrated the following:

- The amplitude of the inwardly propagating pressure wave is increasing. Higher circumferential wave numbers lead to a higher growth rate. The mean flow properties have little effect on the pressure wave propagation.
- The amplitudes of the unsteady circumferential velocity of the impeller wake is decreasing over radius proportional to 1/r regardless of the circumferential wave number and mean flow conditions. The amplitude of the unsteady radial velocity of the impeller wake depends both on the mean flow conditions and the initial wake structure at the impeller exit.

REFERENCES

Bryan, W.B.,1991. An investigation of unsteady impeller-diffuser interactions in a centrifugal compressor, *PhD Dissertation,* Purdue University, Department of Mechanical Engineering.

Drazin P.G., &Reid W.H. 2004, *Hydrodynamic Stability*, Cambridge University Press, United Kingdom, p.69-82

Goldstein, M.E., 1978, Unsteady vertical and entropic distortions of potential flows round arbitrary obstacles, *Journal of Fluid Mechanics*, vol.89, p. 433-468.

Golubev, V. V., & Atassi, H. M., 2000. Unsteady swirling flows in annular cascades, part 1: Evolution of incident disturbances. *AIAA journal*, vol.38, no.7: p. 1142-1149.

Gottfried, D., &Fleeter, S., 2002, Impeller blade unsteady aerodynamic response to vaned diffuser potential fields. *Journal of Propulsion and Power,* vol. 18, no.2 :p. 472-480.

König, S., Petry, N., & Wagner, N. G. 2009. Aeroacoustic Phenomena in High Pressure Centrifugal Compressors— A Possible Root Cause for Impeller Failures. *In Proceedings of the Thirty-Eighth Turbomachinery Symposium.*

Ramakrishnan, K., Richards, S. K., Moyroud, F., & Michelassi, V. ,2011, Multi-Blade Row Interactions in a Low
    Pressure Ratio Centrifugal Compressor Stage With a Vaned Diffuser. *In ASME 2011 Turbo Expo: Turbine
    Technical Conference and Exposition* , p. 1321-1329

Roger, M., 2004, Analytical Modelling of Wake-Interaction Noise in Centrifugal Compressors with Vaned
    Diffusers. *In 10th AIAA/CEAS Aeroacoustics Conference, Manchester* , p. 2994

Smith, S.N.,1971, Discrete Frequency Sound Generation in Axial Flow Turbomachines, *CUED/ATurbo/TR29*

Tyler, J. M.,1962, Axial flow compressor noise studies. *SAE Trans*., vol. 70, p. 309-332.